

Article

Electrochemical Behaviour and Direct Cell Viability Analysis of Hybrid Implants Made of Ti-6Al-4V Lattices Infiltrated with a Bioabsorbable Zn-Based Alloy

Noa Gabay Bass ¹, Galit Katarivas Levy ², Tomer Ron ^{1,*}, Razi Vago ³, Jeremy Goldman ⁴, Amnon Shirizly ¹ and Eli Aghion ¹

¹ Department of Materials Engineering, Ben-Gurion University of the Negev, Beer-Sheva 84105, Israel

² Department of Biomedical Engineering, Ben-Gurion University of the Negev, Beer-Sheva 84105, Israel

³ Department of Biotechnology Engineering, Ben-Gurion University of the Negev, Beer-Sheva 84105, Israel

⁴ Biomedical Engineering Department, Michigan Technological University, Houghton, MI 49931, USA

* Correspondence: toron@post.bgu.ac.il

Abstract: Biodegradable metals are being developed for biomedical implants or components of implants. Biodegradable zinc-based materials, in particular, have been shown to promote bone regeneration in orthopaedic applications. Here, we investigated the potential of a hybrid Ti-Zn system, comprising a Ti-6Al-4V biostable lattice produced by additive manufacturing (AM) infiltrated by a bioabsorbable Zn-2%Fe alloy, to serve as an osseointegrated implant for dental and orthopaedic applications. The osseointegration of implants can be enhanced by a porous implant structure that facilitates bone ingrowth to achieve superior bonding between the bone tissue and the implant. The hybrid material was evaluated in terms of microstructure and localized chemical composition using scanning and transmission electron microscopy with special attention to the interface between the Ti-based lattice and the biodegradable alloy. The electrochemical behaviour of the Ti-Zn system was analysed in a simulated physiological environment in terms of open circuit potential test and cyclic potentiodynamic polarization. Cytotoxicity was evaluated using direct cell viability tests. The results demonstrate desirable properties of the hybrid Ti-Zn system as a non-cytotoxic material with an acceptable corrosion rate.

Keywords: osseointegration; additive manufacturing; SLM; lattice; Ti-6Al-4V; biodegradable zinc; Zn-Fe; orthopaedic; dental



Citation: Gabay Bass, N.; Katarivas Levy, G.; Ron, T.; Vago, R.; Goldman, J.; Shirizly, A.; Aghion, E. Electrochemical Behaviour and Direct Cell Viability Analysis of Hybrid Implants Made of Ti-6Al-4V Lattices Infiltrated with a Bioabsorbable Zn-Based Alloy. *Metals* **2022**, *12*, 1735. <https://doi.org/10.3390/met12101735>

Academic Editors: Reza Parvizi and Anthony Hughes

Received: 24 August 2022

Accepted: 14 October 2022

Published: 16 October 2022

Publisher's Note: MDPI stays neutral with regard to jurisdictional claims in published maps and institutional affiliations.



Copyright: © 2022 by the authors. Licensee MDPI, Basel, Switzerland. This article is an open access article distributed under the terms and conditions of the Creative Commons Attribution (CC BY) license (<https://creativecommons.org/licenses/by/4.0/>).

1. Introduction

For osteointegration to occur, direct contact is essential between an implant and bone tissue during the regenerating process [1–3]. Currently, the most common material for osseointegrated implants is Ti-6Al-4V and other Ti-based alloys, which are selected due to their excellent corrosion resistance, biocompatibility, and low elastic modulus to reduce stress shielding [4–11]. These biostable alloys provide suitable mechanical support and long-term direct contact with bone to support regenerative processes. Additive manufacturing (AM) of Ti-6Al-4V is gaining popularity as an advanced manufacturing technology to produce custom designed fixtures of complex geometry with minimal wasted material [12–16]. In the orthopaedic and dental fields, AM technology enables the production of porous-structured biomedical implants with similar mechanical properties as natural bone. In the implant industry, the immense advantage of AM allows for personalized implants, with control over size, shape, and properties. Furthermore, structural lattices can be infiltrated with a bioabsorbable therapeutic material.

Numerous studies have established the outstanding potential of Zn as a biodegradable metallic material [17–23], with a moderate corrosion rate more consistent with biological healing, as well as reduced risks of undesirable effects common to alternative

Mg- and Fe-based biodegradable metallic materials such as gas embolism (for Mg) and hazardous corrosion products (for Fe) [23–30]. Furthermore, Zn is an important trace element, with relatively high concentrations found in bone, muscle, liver, and skin. It plays a significant role in bone health, improves osteogenesis [31–33], exhibits antibacterial and anti-inflammation properties, and overall plays a significant role in the regulation of the immune system [34–39]. These qualities are appealing in dental and orthopaedic implant applications and may improve the implant performance and reduce post operation complications.

Due to the importance of the Ti alloy for mechanical support and the Zn metal for bioactive therapy to stimulate bone tissue regrowth, we speculated that a hybrid system which combined both materials may be beneficial for orthopaedic applications. However, the corrosion rate of pure Zn may need to be fine-tuned to avoid fibrous encapsulation or the accumulation of stable corrosion products that prevent diffusion at the metal/tissue interface [40]. To increase the corrosion rate, and consequently, the biocompatibility, Zn can be alloyed with other biocompatible materials, such as Fe [41]. In this study, 2%wt Fe was added to pure Zn to create a secondary phase that acts as localized cathodic site to accelerate the corrosion rate. The present study examined the prospect of a hybrid material composed of a Ti-6Al-4V lattice infiltrated with bioabsorbable Zn-2%Fe for osseointegrated implants in in vitro conditions. This study presents further cytotoxicity examinations in terms of direct cell viability as well as microstructural and electrochemical assessments.

2. Materials and Methods

2.1. Preparation of Hybrid Ti-Zn System

The hybrid Ti-Zn system was made from a Ti-6Al-4V lattice produced by additive manufacturing that was subsequently infiltrated by a biodegradable Zn-2%Fe alloy. The Ti-6Al-4V lattice was produced by SLM, using an EOS-EOSINT M280 printer equipped with a 200 W Nd-YAG laser. All the AM lattices were manufactured in the Z-direction and in accordance with ASTM standard 52921-13. The Ti-6Al-4V powder particle size was between 20 and 45 μm with distribution $D_{10} = 24 \mu\text{m}$; $D_{50} = 37 \mu\text{m}$; $D_{90} = 55 \mu\text{m}$. Particle size analysis was carried out using Mastersizer 2000. The laser beam diameter was 60 μm , scanning velocity 7,00 mm/sec, hatch spacing 0.2 mm and the building layer thickness was 30 μm . The SLM scanning direction rotation was 45 degrees and the obtained lattice has a cubic structure with a lattice parameter of 2.5 mm and ribs diameter of 0.9 mm. The biodegradable Zn-2%Fe alloy was produced by gravity casting using pure Zn ingots (99.99%) and pure Fe (99%) powder with a mean grain size of 44 microns. The casting process of Zn-2%Fe was carried out in a graphite crucible in the following steps: (i) remelting of pure Zn at 750 °C; (ii) addition of Fe powder; (iii) stirring every 30 min for 3 h [41]. Notably, the Fe powder was gradually added to the molten zinc while stirring to prevent the floating of the powder on top of the melt surface that can cause undesired oxidation. Prior to the infiltration of the biodegradable Zn alloy, the Ti alloy lattice was pre-heated at 400 °C for 1 h. The infiltration process was carried out by immersing the Ti alloy lattice in molten Zn alloy at a temperature above 700 °C within a steel die. To secure the proper filling of the Ti-based lattice, the infiltration process was accompanied by intensive mechanical shaking.

2.2. Microstructure Examinations

The microstructure of the tested materials was examined using JSM-5600 (Tokyo, Japan) scanning electron microscopy (SEM) integrated with an energy-dispersive X-ray spectroscopy (EDS) [42]. For high resolution observation, transmission electron microscopy (TEM) Electron-transparent cross-section specimens were produced by a dual-beam focused ion beam microscope (FEI, Verios-460 L, Hillsboro, OR, USA). The characterization was carried out using an analytical electron microscope (JEOL JEM-2100F, Jeol Ltd., Tokyo, Japan) operating at 200 kV. This analysis included bright-field (BF) imaging, selected area electron diffraction (SAED), and EDS.

2.3. Electrochemical Behaviour

The electrochemical behaviour of the tested materials was evaluated using a Bio-Logic SP-200 potentiostat equipped with EC-Lab software V11.18. Prior to all electrochemical analyses, the samples were polished to 1200 grit. The tests were carried out in PBS solution using a three-electrode cell that includes a working electrode with an exposed area of 1 cm², a saturated calomel electrode (SCE) as a reference electrode and a platinum counter electrode. The scanning rate of cyclic potentiodynamic polarization analysis was 1 mV/s. Open circuit (OC) analysis was carried out for a duration of 100 h with a sample taken every 10 min.

2.4. Cytotoxicity Testing

Direct cell testing was carried out by evaluating cell viability and adhesion to the hybrid Ti-Zn system's surface. Sample preparation and protocol were carried out according to ISO 0993-5/12 standards [43,44]. The cell viability testing was carried out using *mus musculus* (mouse) 4T1 cells. These cells were cultured in an incubator using Dulbecco Modified Eagle's Medium (DMEM) supplemented with 4.5 g L D-Glucose, 10% Foetal Bovine Serum (FBS), 4 mM L-Glutamine, 1 mM Sodium Pyruvate, and 1% Penicillin Streptomycin Neomycin (PSN) antibiotic mixture (Biological Industry, Beit Haemek, Israel) in a humidified atmosphere with 5% CO₂ at 37 °C. The tests took place in two independent repetitions, each including 4 samples of each alloy (hybrid Ti-Zn system and its components: Zn-2%Fe bioabsorbable alloy and Ti-6Al-4V as a reference alloy). The samples used were of cylindrical shape, with a diameter of 10 mm and a height of 2 mm, polished to 4000 grits. Subsequently, the samples were ultrasonically cleaned for 5 min in ethanol and 2 min in acetone, air-dried, and later sterilized in an autoclave. After a 24 h pre-incubation of the samples in DMEM, they were placed in a 24-well plate. The cells were seeded directly onto the alloys in a density of 100,000 cells per sample and incubated for 2 h in DMEM to allow adhesion. More DMEM was then added to each well according to the standard ratio. The plates were incubated under a humidified atmosphere with 5% CO₂ at 37 °C for 24 and 48 h. The number of adherent cells was visualized using NucBlue™ Live Cell Stain Formulation kit (RHENIUM, Modi'in, Israel) and then documented by a CoolLED pe-2 collimator fitted to an inverted phase-contrast microscope (Eclipse Ti, Nikon) equipped with a digital camera (D5-Qi1Mc, Nikon, Tokyo, Japan) using the appropriate fluorescent filters. Average cell adhesion was calculated by quantifying cells per sq. mm at three random locations for each sample. A Live and Dead Cell Assay (Abcam, Cambridge, UK) was used to evaluate cell viability, following the manufacturer's protocol. The Live and Dead Assay stain solution allows for differentiation between live and dead cells using fluorescent dyes that render viable cells green (Excitation (max) and Emission (max) are 494 nm and 515 nm, respectively) and cells with compromised plasma membranes red (excitation (max) and emission (max) are 528 nm and 617 nm, respectively).

3. Results

The general appearance of the Ti-6Al-4V lattice obtained by the SLM process is shown in Figure 1a. This illustrates the symmetric cubic structure of the lattice as well as the locations of open spaces identified as darker areas. A close-up view of the Ti-based lattice infiltrated with bioabsorbable Zn-2%Fe alloy is shown in Figure 1b. This clearly demonstrates that the infiltrated alloy was able to penetrate and fill the open spaces within the lattice with coherent connection to the internal titanium structure.

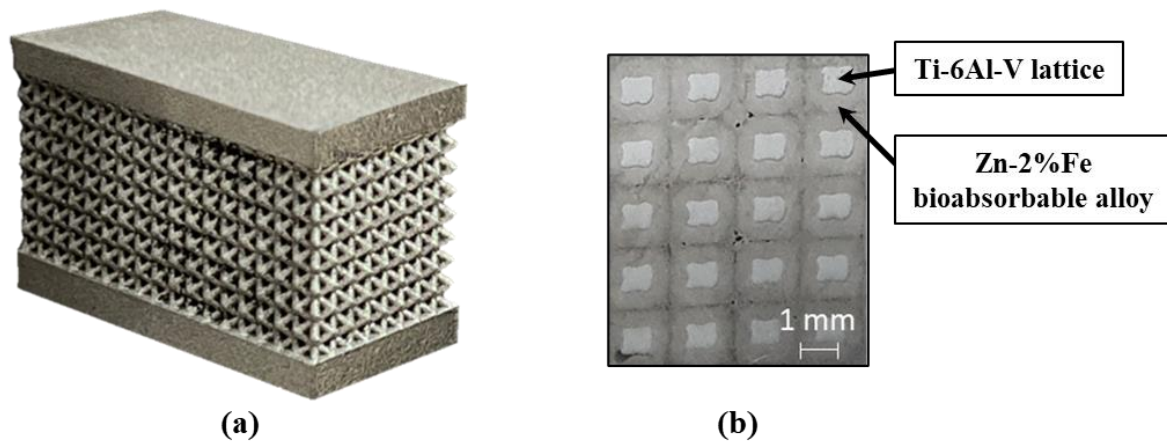


Figure 1. General appearance of (a) Ti-6Al-4V lattice pre-infiltration; (b) close-up view of Ti-6Al-4V lattice post-infiltration.

Close-up view of the boundary between the Ti-based lattice and the infiltrated Zn-2%Fe alloy as obtained by SEM back-scatter electron (BSE) imaging is shown in Figure 2. An EDS analysis was performed for the different identified areas as shown in Table 1: The first data point refers to a Zn-rich area, with a low number of Ti-6Al-4V components, which is assumed to comprise a Zn matrix and $Zn_{11}Fe$ according to Kafri et al. [42]. The second data point refers to an area with large amounts of Zn along with a significant amount of the Ti alloy's components and a lower Fe percentage, with a composition of $TiZn_3$ [41]. Data point number 3 refers to the interface layer approximately 100 μm from the Ti-based lattice's edge, which can be identified in a close-up view shown in Figure 2b. It comprises a significant amount of Ti, Al, and V, along with approximately 3.5% at of Fe, which suggests both $TiZn_3$ and a ferritic phase are present. The 4th data point refers to the Ti-based lattice, which, as expected, mainly contains the elements Ti, Al and V, with very small amounts of Zn and Fe, which can be attributed to the large interaction volume of SEM EDS that could acquire a signal from deeper areas of the sample. The microstructure of Ti-6Al-4V lattice produced by SLM was composed of fine metastable martensitic α' phase and small amounts of β phase [45]. The martensitic phase actually substitutes the regular α phase that is obtained in slower cooling rates at regular casting conditions.

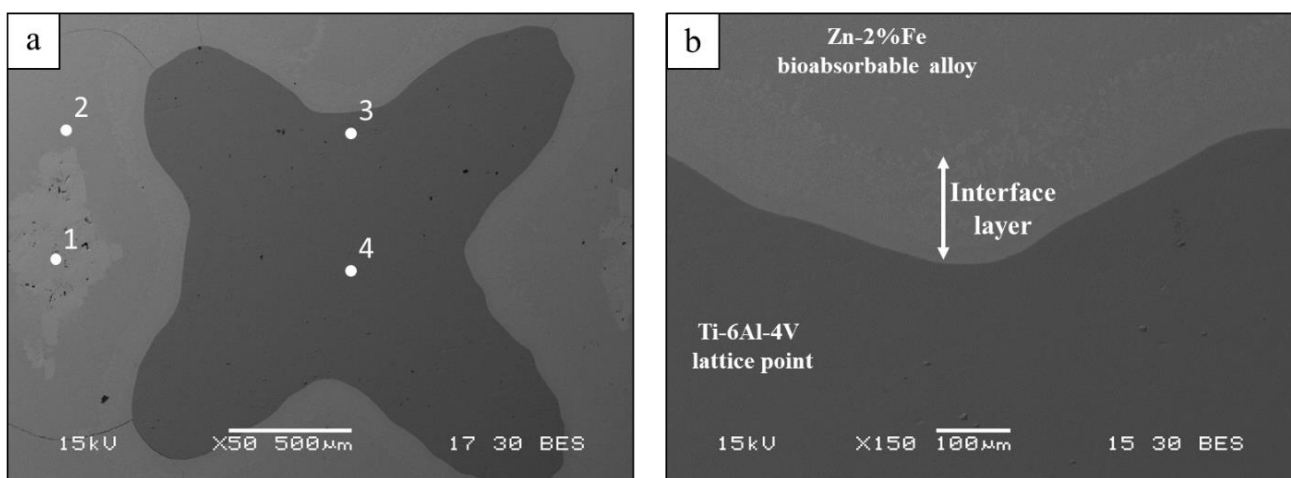
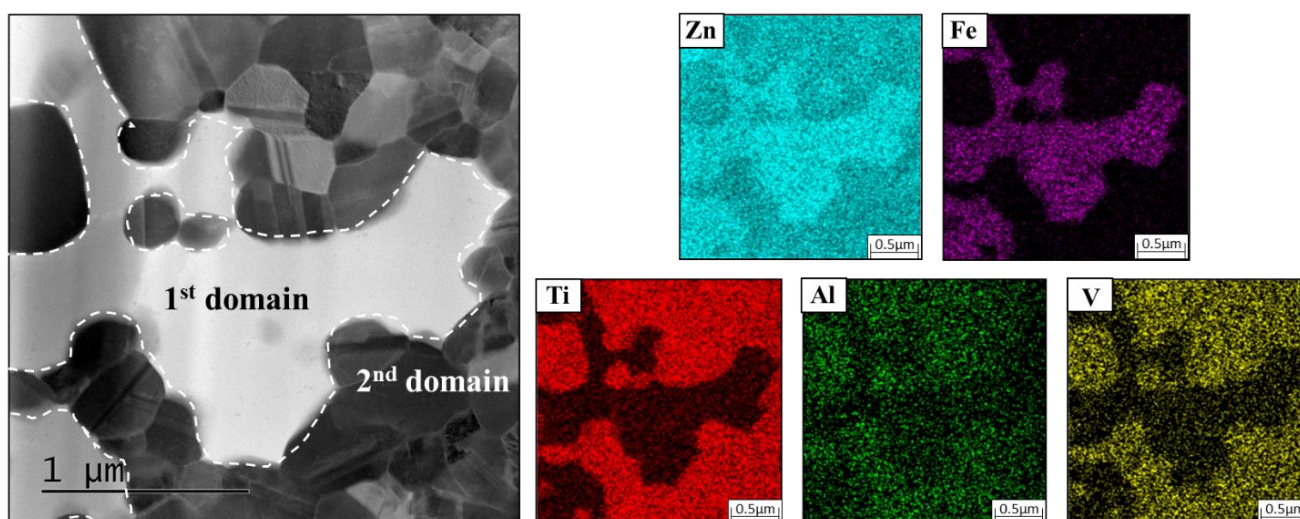


Figure 2. Microstructure of hybrid Ti-Zn system by SEM (a) points of EDS measurements (b) Close-up view at the interface between Ti-based lattice and Zn-based alloy.

Table 1. Spot chemical compositions (at%) by EDS at points shown in Figure 2a.

Point of Measurement	Zn	Fe	Ti	Al	V	Dominant Phases [27,41,45]
1	89.72 ± 5.1	5.88 ± 4.7	3.82 ± 0.9	0.55 ± 0.5	0.03 ± 0.06	Zn + Zn ₁₁ Fe
2	73.67 ± 0.9	0.54 ± 0.6	23.2 ± 1.3	1.62 ± 0.3	1.62 ± 0.3	TiZn ₃
3	78.58 ± 0.4	3.4 ± 0.13	16.32 ± 0.2	1.02 ± 0.1	1.02 ± 0.1	TiZn ₃ + Zn ₁₁ Fe
4	0.18 ± 0.1	0.15 ± 0.05	88.66 ± 0.3	7.39 ± 0.1	3.62 ± 0.1	Ti (α' + β)

A TEM sample was taken from the interface layer, within up to 100 μm from the Ti-based lattice's edge as shown in Figure 3. BF and EDS analyses concluded that the interface layer was composed of two main domains: large grains with increased amount of Ti-6Al-4V alloy ingredients and small grains with relatively reduced content of Ti-6Al-4V alloy ingredients and increased amounts of Fe, as shown in Table 2.

**Figure 3.** TEM-BF close-up view of the interface layer between the Ti-based lattice and Zn-2%Fe alloy along with chemical composition maps of elements in each domain obtained by STEM-EDS analysis.**Table 2.** Composition (at%) of grains of each domain located at the interface layer as obtained by STEM EDS.

Domain	Zn	Fe	Ti	Al	V
Large grains (light grey)	70.8	0.4	25.3	2.4	1.1
Small Grains (dark grey)	85.1	8.7	5.8	0.4	0.1

The two domains were further investigated to determine the phases present in each domain. SAED analyses of each domain are presented in Figure 4. Each domain was composed of one dominant phase. The first domain, with elevated amounts of Ti-6Al-4V components, was identified as an intermetallic ternary Ti-Fe-Zn phase [46]. This is supported by Gross et al. [47], as the identified phase is of CeCr₂Al₂₀-type structure, possibly based on ZrFe₂Zn₂₀ Fd-3m structure ($a = 1.3955$ nm), where the Zr sites are replaced with Ti atoms, which share the same column in the periodic table, to create TiFe₂Zn₂₀ with a ≈ 1.4 nm. The second domain was identified as TiZn₃, Pm-3m ($a = 0.39322$ nm), as anticipated.

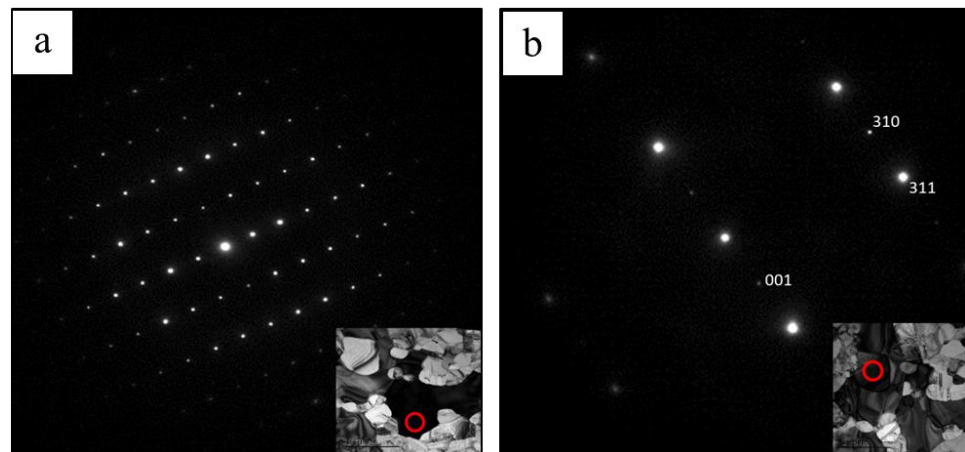


Figure 4. SAED analysis of the first and second domains as marked with red circles (a,b).

The cyclic potentiodynamic polarization analysis of the hybrid Ti-Zn system and Zn-2%Fe alloy is shown in Figure 5. The corrosion current of the hybrid system was relatively increased compared with the Zn-based alloy (2.4 [μA] vs. 0.3 [μA], respectively) along with an increased corrosion rate ($3.6 \cdot 10^{-2}$ vs. $0.5 \cdot 10^{-2}$ [mmpy]), as presented in Table 3. The increased corrosion of the hybrid system mainly relates to galvanic corrosion attack that takes place between the cathodic Ti-matrix lattice and the Zn-based alloy. In addition, the protection potential (E_{pp}) path in the case of the Zn-based alloy crosses the anodic branch above the E_{corr} , while the E_{pp} path of the hybrid system crosses the cathodic branch below the E_{corr} . According to Peter et al. [48] and Stansbury et al. [49], this means that while the Zn-based alloy is generally sensitive to localized corrosion attack, the hybrid system undergoes pitting corrosion at surface defects. In our case, the surface defects in the hybrid system are the interfaces between the Ti-matrix lattice and the infiltrated biodegradable Zn-based alloy.

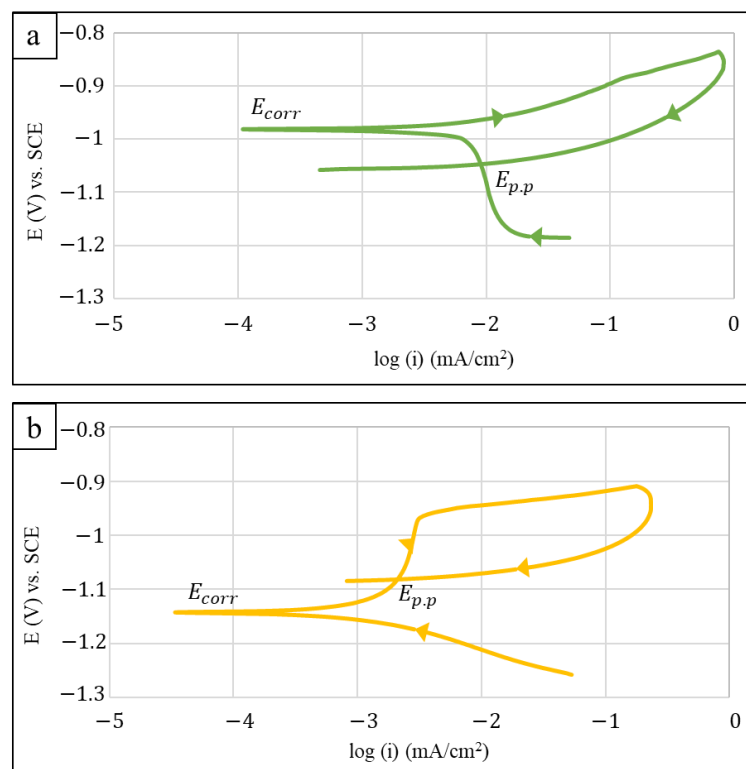
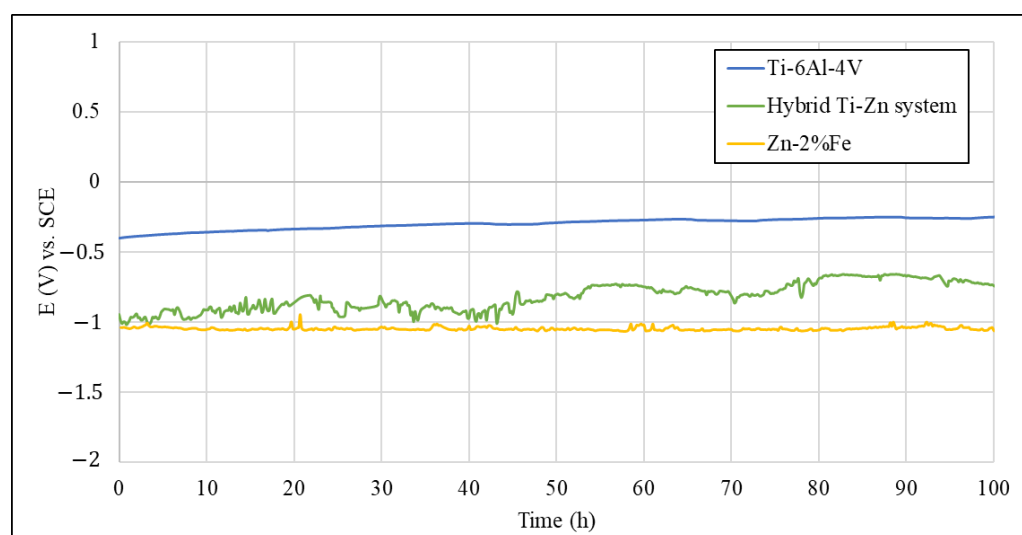


Figure 5. Cyclic potentiodynamic polarization analysis in PBS solution (a) hybrid Ti-Zn system (b) Zn-2%Fe alloy.

Table 3. Results obtained by Tafel extrapolation.

Sample	E_{corr} (V) vs. SCE	I_{corr} (μA)	C.R. (mmpy)	$E_{\text{p,p}}$ (V) vs. SCE
Hybrid Ti-Zn system	-0.982 ± 0.001	2.4 ± 1.2	0.036 ± 0.018	-1.06 ± 0.01
Zn-2%Fe	-1.134 ± 0.008	0.3 ± 0.1	0.005 ± 0.002	-1.12 ± 0.04

A further electrochemical behaviour examination was carried out using open circuit analysis of the hybrid system compared with its separate alloys, as shown in Figure 6 and Table 4. The results demonstrate that the open circuit potential of the hybrid material falls between the open circuit potential of its two constituent materials. Furthermore, the potential of the hybrid system is less stable than the Zn-based alloy that experiences the corrosion. This can be attributed to the micro-galvanic effect between the absorbable alloy and the Ti-based lattice, which makes the Zn-based alloy more prone to corrosion.

**Figure 6.** Open circuit potential analysis of hybrid Ti-Zn system and its constituent materials.**Table 4.** Open circuit potential measurements with statistical deviations as obtained after 100 h of immersion.

Sample	E_{corr} (V) vs. SCE
Ti-6Al-4V	-0.30 ± 0.04
Hybrid Ti-Zn system	-0.81 ± 0.10
Zn-2%Fe	-1.05 ± 0.01

Direct cytotoxicity analysis of Hybrid Ti-Zn system was carried out following incubation periods of 24 h and 48 h, as shown in Figure 7. The ability of cells to adhere to the alloys and their viability provide critical information regarding the biocompatibility of the experimental hybrid implant material. We found an increase of almost 100% in cell amount from 24 to 48 h of incubation for all the tested alloys, as shown in Figure 8. The smaller number of cells in the hybrid Ti-Zn system of 72 and 134 cells/field after 24 and 48 h, respectively can be attributed to the uneven surface of the samples. This was due to accelerated inhomogeneous corrosion of the bioabsorbable alloy in the hybrid system, which interfered with the cell seeding process. Cells usually prefer uneven surfaces; thus, the rugged surface of the biodegradable alloy should enhance adhesion. Nonetheless, the results showed a reduced number of adhered cells that can also be attributed to low field depth of the microscope with inability to observe different surface heights simultaneously.

Notably, the number of adhered cells to the hybrid material has nearly the same magnitude as in the case of the inert Ti-6Al-4V that was used as positive control (140 and 215 cells/field, respectively), and therefore showed promising prospects. In comparison, the Zn-2%Fe alloy by itself has a cell count of 188 and 380 cells/field after 24 and 48 h that exceeded both the Ti-6Al-4V and Ti-Zn system, which implies that this alloy promotes cell multiplication and adhesion, as desired for bone implant applications. Those findings were basically in accordance with the observations of Avior et al. [28].

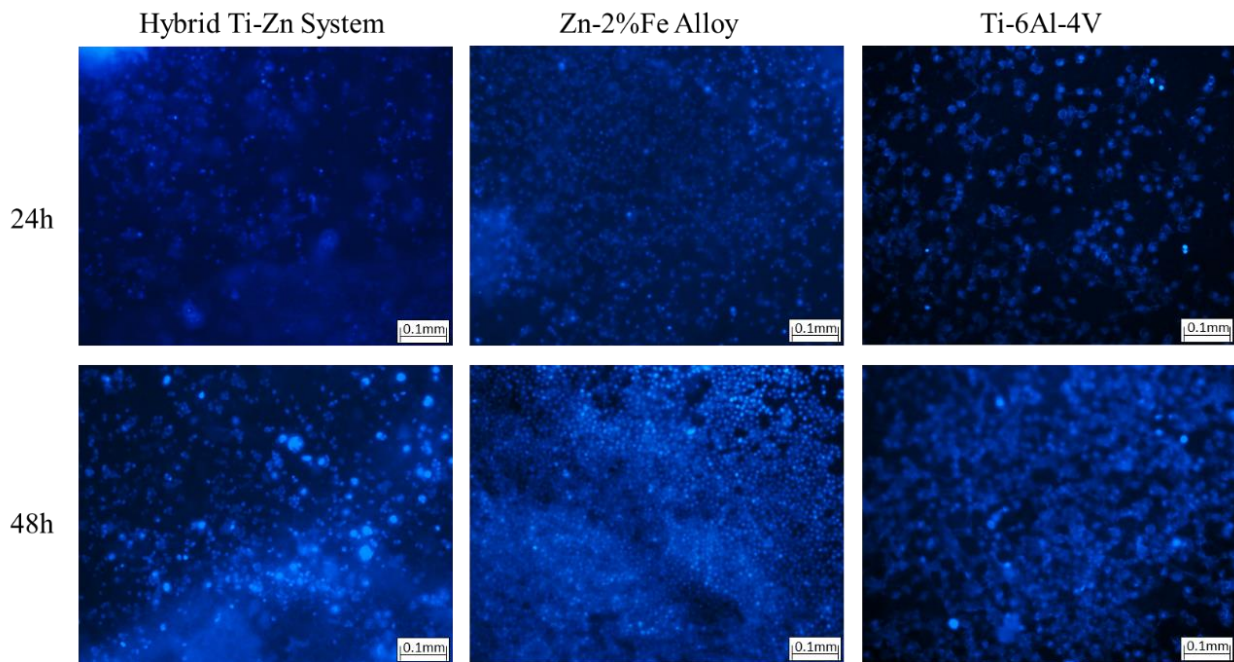


Figure 7. Fluorescence images of NucBlue-stained 4T1 cells attached to the surface of the corresponding alloys after 24 and 48 h of incubation. Scalebar = 100 μ m.

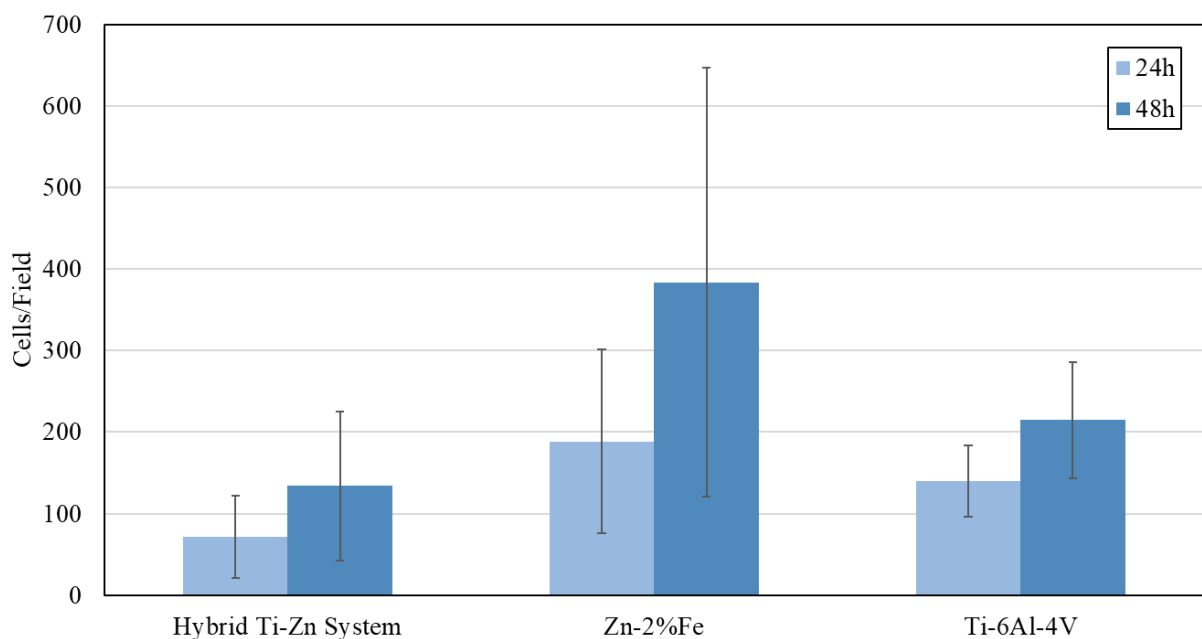


Figure 8. Cell count of 4T1 cells per unit field after 24 h and 48 h incubation while adhered to the alloys' surfaces.

In addition to cell adherence, cell viability was assessed to determine the cytotoxicity of the tested materials. In terms of cell viability, the adhered cell viability was tested using a Live and Dead Cell Assay, as shown in Figure 9. For cells adhered to both the hybrid Zn-Ti system and the Zn-based alloy, a relatively small amount of the cells is tinted red, which suggests that their plasma membranes are compromised, while most of the cells were alive. This demonstrates that the alloys investigated have acceptable biocompatibility in direct contact in vitro conditions.

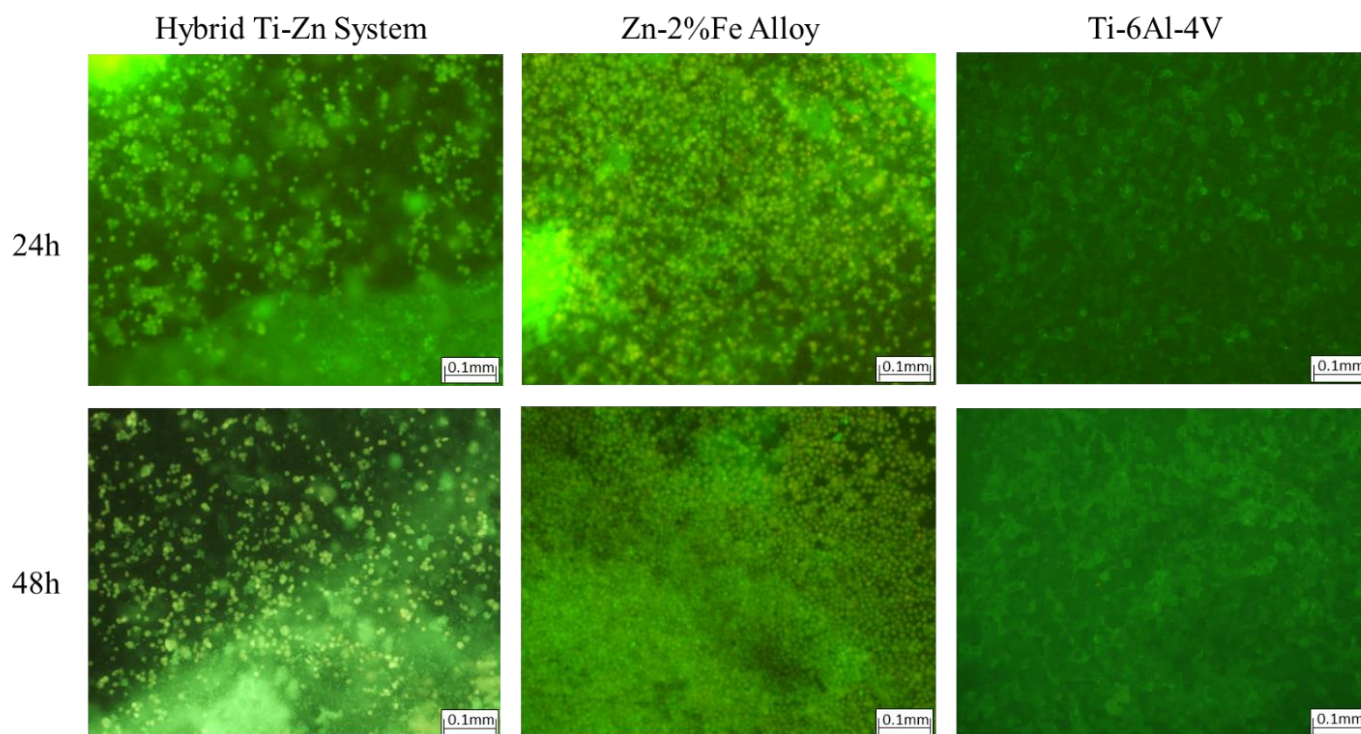


Figure 9. Fluorescence images of live (green) and dead (red) 4T1 cells attached to the corresponding alloys after 24 and 48 h of incubation. Scalebar = 100 μ m.

4. Discussion

Zn-based bioabsorbable implants are gaining popularity due to zinc's biocompatibility, potential bone growth stimulation and anti-inflammatory properties, in addition to dissolvability in a biological environment. The main corrosion products of Zn are $Zn(OH)_2$ and ZnO that are converted in the physiological environment to soluble chloride salts that can be efficiently excreted from the body through the kidneys, preventing cytotoxicity. Furthermore, Ti-based alloys, particularly Ti-6Al-4V, are commonly used as biostable structural material for high-load implants in orthopaedic and dental applications. Here, a hybrid Ti-Zn system is proposed as an attractive material for osseointegrated implants [1,3], combining the advantages of the two constituent materials. The promise of the hybrid material is the combination of structural support with high porosity and bone growth, stimulating zinc degradation products to encourage rapid and strong interfacial bonding between the Ti support and regenerating bone tissue [30]. A key advantage of our approach for combining the two metals into the hybrid system is that the Ti support can be further refined to tailor the mechanical properties and porosity to optimize interfacial bonding. In parallel, the zinc-based material can be independently engineered through alloying to fine-tune its corrosion rate and release of therapeutic corrosion by products to stimulate bone regrowth more optimally.

Biocompatibility is essential for a potential implant material, which must allow the adhesion of cells to the surface to promote healthy tissue regrowth both within and around the implant. In an earlier study, the hybrid Ti-Zn system showed desirable biocompatibility

in terms of indirect cell viability, with adequate corrosion rate and mechanical integrity [40]. The present study further demonstrates the Ti-Zn system has adequate biocompatibility in terms of direct contact viability between the cells and the hybrid material surface. This comes in addition to adequate adhesion between the tested cells and the Ti-Zn system, and coherent adhesion between the constituent Ti-based and Zn-based alloys. The acceptable attachment and viability of cells on the surface of the hybrid system suggests that cells will be able to migrate within the pores of the implant as the impregnated zinc alloy bio corrodes over time. Based on the present results, the biocompatibility of this experimental hybrid material should be further investigated in in vivo studies to confirm the ability of bone forming cells to migrate into and remain viable within the porous structure, as well as to generate strong interfacial bonding with the regenerating bone tissue.

We showed that a ternary intermetallic phase is formed within the 100 μm interface layer in addition to TiZn_3 phase further from the interface between the alloys. This reveals a strong bond, which was also demonstrated previously [27] in terms of compression tests. For the implant to perform appropriately, there must be a strong bond between the lattice and infiltrating alloy. A strong interfacial bond between implant constituents allows for the implant to be remain intact during deployment and while functioning under high loads.

In the current and previous studies, the Ti-Zn system exhibited desirable electrochemical properties, with an accelerated corrosion rate compared with pure Zn [41] that is intended to prevent fibrous encapsulation responses. As demonstrated by cyclic potentiodynamic polarization, the hybrid material experiences corrosion via defects and pitting. The Zn-alloy, as expected, dissolves in a simulated physiological environment, leaving an exposed Ti-based lattice with cavities within which healthy tissue can regenerate. An acceptable time for complete dissolution of the Zn-based alloy should be approximately 12 months as in the case of biodegradable polymers. In parallel, the increased corrosion rate should not affect the mechanical performance of the Ti-based lattice structure and refers only to the infiltrated biodegradable alloy. Moreover, in previous research [27], it was demonstrated that a bare lattice could withstand compressive load with a yield point of above 397 MPa. The corrosion rate could be controlled to match the rate of tissue regeneration by tuning the Ti-Zn surface area ratio to produce lattices with varying densities and geometries to accommodate the physiological needs.

5. Conclusions

- i. The hybrid Ti-Zn system in the form of Ti-6Al-4V lattice infiltrated with bioabsorbable Zn-2%Fe alloy, demonstrates acceptable direct cell viability and adhesion in in vitro conditions.
- ii. The hybrid system exhibits adequate electrochemical behaviour and dissolvability in a simulated physiological environment that were partly related to the micro galvanic effect generated between the Ti-based lattice and the biodegradable alloy.
- iii. The ternary phase found at the interface between the Ti lattice and Zn-2%Fe alloy via TEM BF and SAED suggests a strong bond between the Ti-based lattice and the infiltrating Zn-based alloy, which further reinforces the attractiveness of the hybrid system as a bone implant material.

Author Contributions: N.G.B.: investigation, formal analysis, and writing—original draft; G.K.L.: investigation; T.R.: investigation; R.V.: investigation; J.G.: investigation; A.S.: investigation, supervision; E.A.: conceptualization, methodology, supervision, and writing—original draft. All authors have read and agreed to the published version of the manuscript.

Funding: This research received no external funding.

Informed Consent Statement: Not applicable.

Data Availability Statement: Experimental data from this study are available from the corresponding author upon reasonable request.

Conflicts of Interest: The authors declare no conflict of interest.

References

1. Albrektsson, T.; Zarb, G.A. Current interpretations of the osseointegrated response: Clinical significance. *Int. J. Prosthodont.* **1993**, *6*, 95–105.
2. Matos, G.R.M. Surface Roughness of Dental Implant and Osseointegration. *J. Maxillofac. Oral Surg.* **2021**, *20*, 1–4. [[CrossRef](#)]
3. Adell, R.; Eriksson, B.; Lekholm, U.; Brånemark, P.I.; Jemt, T. A Long-Term Follow-up Study of Osseointegrated Implants in the Treatment of Totally Edentulous Jaws. *Int. J. Oral Maxillofac. Implant.* **1990**, *5*, 347–359.
4. Wang, K. The use of titanium for medical applications in the USA. *Mater. Sci. Eng. A* **1996**, *213*, 134. [[CrossRef](#)]
5. Lewallen, E.A.; Riester, S.M.; Bonin, C.A.; Kremers, H.M.; Dudakovic, A.; Kakar, S.; Cohen, R.C.; Westendorf, J.J.; Lewallen, D.G.; van Wijnen, A.J. Biological strategies for improved osseointegration and osteoinduction of porous metal orthopedic implants. *Tissue Eng. Part B Rev.* **2015**, *21*, 218–230. [[CrossRef](#)]
6. Sovak, G.; Weiss, A.; Gotman, I. Osseointegration of Ti6Al4V alloy implants coated with titanium nitride by a new method. *J. Bone Jt. Surg.* **2000**, *82*, 290–296. [[CrossRef](#)]
7. John, A.A.; Jaganathan, S.K.; Supriyanto, E.; Manikandan, A. Surface Modification of Titanium and Its Alloys for the Enhancement of Osseointegration in Orthopaedics. *Curr. Sci.* **2016**, *111*, 1003–1015. [[CrossRef](#)]
8. Long, M.; Rack, H. Titanium alloys in total joint replacement—A materials science perspective. *Biomaterials* **1998**, *19*, 1621. [[CrossRef](#)]
9. Niinomi, M. Mechanical properties of biomedical titanium alloys. *Mater. Sci. Eng. A* **1998**, *243*, 243. [[CrossRef](#)]
10. Spriano, S.; Yamaguchi, S.; Baino, F.; Ferraris, S. A critical review of multifunctional titanium surfaces: New frontiers for improving osseointegration and host response, avoiding bacteria contamination. *Acta Biomater.* **2018**, *79*, 1–22. [[CrossRef](#)]
11. Head, W.C.; Bauk, D.J.; Emerson, R.H., Jr. Titanium as the material of choice for cementless femoral components in total hip arthroplasty. *Clin. Orthop.* **1995**, *311*, 85–90.
12. Cui, C.; Hu, B.; Zhao, L.; Liu, S. Titanium alloy production technology, market prospects and industry development. *Mater. Des.* **2011**, *32*, 1684–1691. [[CrossRef](#)]
13. Yan, C.; Hao, L.; Hussein, A.; Young, P. Ti–6Al–4V triply periodic minimal surface structures for bone implants fabricated via selective laser melting. *J. Mech. Behav. Biomed. Mater.* **2015**, *5*, 61–73. [[CrossRef](#)]
14. Liu, S.; Shin, Y.C. Additive manufacturing of Ti6Al4V alloy: A review. *Mater. Des.* **2019**, *164*, 107552. [[CrossRef](#)]
15. Van Bael, S.; Kerckhofs, G.; Moesen, M.; Pyka, G.; Schrooten, J.; Kruth, J.P. Micro-CT-based improvement of geometrical and mechanical controllability of selective laser melted Ti6Al4V porous structures. *Mater. Sci. Eng. A* **2011**, *528*, 7423–7431. [[CrossRef](#)]
16. Harun, W.S.W.; Manam, N.S.; Kamariah, M.S.I.N.; Sharif, S.; Zulkifly, A.H.; Ahmad, I.; Miura, H. A review of powdered additive manufacturing techniques for Ti-6Al-4V biomedical applications. *Powder Technol.* **2018**, *331*, 74–97. [[CrossRef](#)]
17. Fraker, A.C.; Ruff, A.W. Metallurgical Surgical Implants State of the Art. *JOM* **1977**, *29*, 2–28. [[CrossRef](#)]
18. Zakay, A.; Aghion, E. Effect of post-heat treatment on the corrosion behavior of AlSi10Mg alloy produced by additive manufacturing. *JOM* **2019**, *71*, 1150–1157. [[CrossRef](#)]
19. Kubásek, J.; Vojtěch, D.; Jablonská, E.; Pospíšilová, I.; Lipov, J.; Ruml, T. Structure, mechanical characteristics and in vitro degradation, cytotoxicity, genotoxicity, and mutagenicity of novel biodegradable Zn–Mg alloys. *Mater. Sci. Eng. C* **2016**, *58*, 24–35. [[CrossRef](#)] [[PubMed](#)]
20. Venezuela, J.; Dargusch, M.S. The influence of alloying and fabrication techniques on the mechanical properties, biodegradability and biocompatibility of zinc: A comprehensive review. *Acta Biomater.* **2019**, *87*, 1–40. [[CrossRef](#)]
21. Sykaras, A.M.; Iacopino, V.A.; Marker, R.G.; Triplett, R.D. Woody, Implant materials, designs, and surface topographies their effect on osseointegration. A literature review. *Int. J. Oral Maxillofac. Implant.* **2000**, *15*, 675–690.
22. Manam, N.S.; Harun, W.S.W.; Shri, D.N.A.; Ghani, S.A.C.; Kurniawan, T.; Ismail, M.H.; Ibrahim, M.H.I. Study of corrosion in biocompatible metals for implants a review. *J. Alloys Compd.* **2017**, *701*, 698–715. [[CrossRef](#)]
23. García-Mintegui, C.; Cordoba, L.C.; Buxadera-Palomero, J.; Marquina, A.; Jimenez-Pique, E.; Ginebra, M.P.; Cortina, J.L.; Pegueroles, M. Zn-Mg and Zn-Cu alloys for stenting applications: From nanoscale mechanical characterization to in vitro degradation and biocompatibility. *Bioact. Mater.* **2021**, *6*, 4430–4446. [[CrossRef](#)]
24. Levy, G.K.; Goldman, J.; Aghion, E. The prospects of zinc as a structural material for biodegradable implants—Review paper. *Metals* **2017**, *7*, 402. [[CrossRef](#)]
25. Aghion, E.; Yered, T.; Perez, Y.; Gueta, Y. The prospects of carrying and releasing drugs via biodegradable magnesium foam. *Adv. Biomater.* **2010**, *12*, B374–B379. [[CrossRef](#)]
26. Kabir, H.; Munir, K.; Wen, C.; Li, Y. Recent research and progress of biodegradable zinc alloys and composites for biomedical applications: Biomechanical and biocorrosion perspectives. *Bioact. Mater.* **2021**, *6*, 836–879. [[CrossRef](#)]
27. Gabay, N.; Ron, T.; Vago, R.; Shirizly, A.; Aghion, E. Evaluating the Prospects of Ti-Base Lattice Infiltrated with Biodegradable Zn–2%Fe Alloy as a Structural Material for Osseointegrated Implants—In Vitro Study. *Materials* **2021**, *14*, 4682. [[CrossRef](#)]
28. Avior, O.; Ghedalia-Peled, N.B.; Ron, T.; Goldman, J.; Vago, R.; Aghion, E. Stress Corrosion Analysis and Direct Cell Viability of Biodegradable Zn-Fe-Ca Alloy in In-Vitro Conditions. *Metals* **2022**, *12*, 76. [[CrossRef](#)]
29. Hui, Q.; Yao-chao, Z.; Zhi-quan, A.; Meng-qi, C.; Qi, W.; Tao, C.; Qiao-jie, W.; Jia-xing, W.; Yao, J.; Xian-long, Z.; et al. Enhanced antibacterial properties, biocompatibility, and corrosion resistance of degradable Mg–Nd–Zn–Zr alloy. *Biomaterials* **2015**, *53*, 211–220.

30. Perets, T.; Ghedalia-Peled, N.B.; Vago, R.; Goldman, J.; Shirizly, A.; Aghion, E. In vitro behavior of bioactive hybrid implant composed of additively manufactured titanium alloy lattice infiltrated with Mg-based alloy. *Mater. Sci. Eng. C* **2021**, *129*, 112418. [[CrossRef](#)]
31. Yusa, K.; Yamamoto, O.; Iino, M.; Takano, H.; Fukuda, M.; Qiao, Z. Eluted zinc ions stimulate osteoblast differentiation and mineralization in human dental pulp stem cells for bone tissue engineering. *Arch. Oral Biol.* **2016**, *71*, 162–169. [[CrossRef](#)] [[PubMed](#)]
32. Wang, S.; Li, R.; Xia, D.; Zhao, X.; Zhu, Y.; Gu, R.; Yoon, J.; Liu, Y. The impact of Zn-doped synthetic polymer materials on bone regeneration: A systematic review. *Stem Cell Res. Ther.* **2021**, *12*, 123. [[CrossRef](#)] [[PubMed](#)]
33. Neščáková, Z.; Zheng, K.; Liverani, L.; Nawaz, Q.; Galusková, D.; Kaňková, H. Multifunctional zinc ion doped sol-gel derived mesoporous bioactive glass nanoparticles for biomedical applications. *Bioact. Mater.* **2019**, *4*, 312–321. [[CrossRef](#)] [[PubMed](#)]
34. Favier, A.; Favier, M. Effects of zinc deficiency in pregnancy on the mother and the newborn infant. *Rev. Fr. Gynecol. Obstet.* **1990**, *85*, 13–27. [[PubMed](#)]
35. Gammoh, N.Z.; Rink, L. Zinc in Infection, and Inflammation. *Nutrients* **2017**, *9*, 624. [[CrossRef](#)]
36. Haase, H.; Rink, L. Multiple impacts of zinc on immune function. *Metall. Integr. Biomet. Sci.* **2014**, *6*, 1175–1180. [[CrossRef](#)]
37. Mills, C.F. (Ed.) Zinc in Human Biology. In *Physiology of Zinc: General Aspects*; Springer: London, UK, 1989.
38. Prasad, A.S. Zinc: Role in immunity, oxidative stress and chronic inflammation. *Curr. Opin. Clin. Nutr. Metab. Care* **2009**, *12*, 646–652. [[CrossRef](#)]
39. Wong, C.P.; Ho, E. Zinc and its role in age-related inflammation and immune dysfunction. *Mol. Nutr. Food Res.* **2012**, *56*, 77–87. [[CrossRef](#)]
40. Drelich, A.J.; Zhao, S.; Guillory, R.J.; Drelich, J.W.; Goldman, J. Long-term surveillance of zinc implant in murine artery: Surprisingly steady biocorrosion rate. *Acta Biomater.* **2017**, *58*, 539–549. [[CrossRef](#)]
41. Kafri, A.; Ovadia, S.; Goldman, J.; Drelich, J.; Aghion, E. The Suitability of Zn–1.3%Fe Alloy as a Biodegradable Implant Material. *Metals* **2018**, *8*, 153. [[CrossRef](#)]
42. Kaya, A.; Uzan, P.; Eliezer, D.; Aghion, E. Electron microscopical investigation of as cast AZ 91 D alloy. *Mater. Sci. Technol.* **2000**, *16*, 1001–1006. [[CrossRef](#)]
43. ISO Central Secretaria. 2009. Available online: <https://www.iso.org/standard/36406.html> (accessed on 28 April 2021).
44. ISO-10993-5; Biological Evaluation of Medical Devices, Part 5: Tests for In Vitro Cytotoxicity. International Organization for Standardization: Cham, Switzerland, 2009.
45. Leon, A.; Levy, G.K.; Ron, T.; Shirizly, A.; Aghion, E. The effect of hot isostatic pressure on the corrosion performance of Ti-6Al-4V produced by an electron-beam melting additive manufacturing process. *Addit. Manuf.* **2020**, *33*, 101039.
46. Tang, X.; Yin, F.; Wang, X.; Wang, J.; Su, X.; Tang, N.Y. The 450 °C Isothermal Section of the Zn-Fe-Ti System. *JPEDAV* **2007**, *28*, 355–361. [[CrossRef](#)]
47. Gross, N.; Nasch, T.; Jeitschko, W. Ternary Intermetallics with High Zinc Content: TT'2Zn20 (T 5Zr, Hf, Nb; T'=Mn, Fe, Ru, Co, Rh, Ni) with CeCr2Al20-Type Structure. *J. Solid-State Chem.* **2001**, *161*, 288–293. [[CrossRef](#)]
48. Peter, W.H.; Buchanana, R.A.; Liub, C.T.; Liawa, P.K.; Morrisona, M.L.; Hortonb, J.A.; Carmichael, C.A., Jr.; Wrightb, J.L. Localized corrosion behavior of a zirconium-based bulk metallic glass relative to its crystalline state. *Intermetallics* **2002**, *10*, 1157–1162. [[CrossRef](#)]
49. Stansbury, E.E.; Buchanan, R.A. *Fundamentals of Electrochemical Corrosion*; ASM International: Novelty, OH, USA, 2000.